Computing the one-dimensional model of an electron scattered by a quantum junction

Author: Eric Vidal **Supervisor**: Alain Dereux

1 Introduction

The main goal of this project is to numerically understand and show the power of the algorithm for solving systems of N linear equations with N unknowns. It is widely known that the deeply studied linear equation solver is the most stable algorithm of scientific computing. Therefore, whenever it is possible to cast a physical problem into a system of linear equations, one should do it relying on the lower-upper factorization of a $N \times N$ matrix.

For this work, the study case generates the numerical solutions of one-dimensional scattering quantum states given a time-independent potential with an arbitrary shape, $U(x)$. Hence, the PDE to take into account is the 1D time-dependent Schrödinger equation,

$$-\frac{\hbar}{2m}\frac{\partial^2\psi(x,t)}{\partial x^2} + U(x)\psi(x,t) = i\hbar\frac{\partial\psi(x,t)}{\partial t} \tag{1}$$

where the time-independent potential term is applied, and m is the mass of the quantum system considered, which in this work is the electron mass, m_e.

It is important to mention that the physical approach to this problem leads us to consider that the system's extent is larger than the De Broglie wavelength of the electron. Plus, the nonzero region of the potential is comparable with the wavelength consisting of a localized potential.

At this point, one can perform a separation of variables, $\psi(x,t) = \phi(x)\tau(t)$, with the initial condition $\psi(x,t=0) = f(x)$. On the one hand, this leads to solving a basic ODE for the time-dependent term with a solution, $\tau(t) = \alpha_\omega e^{-i\omega t}$ where we have defined the dispersion relation,

$$\omega_0 = \frac{E}{\hbar} = \frac{\hbar k^2}{2m}. \tag{2}$$

measured in Hz.

On the other hand, one finds the eigenvalue equation which can be cast as a one-dimensional Helmholtz equation,

$$\frac{d^2\phi(x)}{dx^2} + k^2\phi(x) = V(x)\phi(x) \tag{3}$$

where it is defined $k^2 = \frac{2mE}{\hbar^2}$ and $V(x) = \frac{2mU(x)}{\hbar^2}$.

Eventually, the initial PDE has been split into 2 ODEs, the temporal one, and the spatial one, which is given by a one-dimensional Lippman-Schwinger integral equation that generalizes (3),

$$\phi(x) = \phi_0(x) + \phi_s(x) = \phi_0(x) + \int dx' G_0(x,x';k)v(x')\phi(x') \tag{4}$$

where $\phi_s(x)$ is the scattered field, $\phi_0(x)$ is the incident field solution of the Helmholtz equation with $V(x) = 0$, $\phi_0(x) = A_k e^{ikx}$, and $G_0(x,x';k)^*$ is determined by,

$$\frac{d^2G_0(x,x';k)}{dx^2} + k^2G_0(x,x';k) = \delta(x-x'). \tag{5}$$

Finally, with these equations, one can find the scattering eigenstates by using a discretized potential, W, and a discretized Green's function, G^0, that results in the following $N \times N$ system of linear equations,

$$[\mathbb{I} - G^0_{A,A}W_{A,A}]|\phi_A\rangle = |\phi_A\rangle, \tag{6}$$

set to apply the algorithm for linear equation systems.

The Green's function that is ruled by (5) is almost a homogeneous differential equation except for the Dirac delta function which adds an inhomogeneous character. This discontinuity is solved by a term proportional to a Heaviside step function.

2 Methods

In what concerns the physical meaning of the problem, the essential target of the work is to compute the Resonant Tunneling devices in GaAs-AlGaAs heterostructures. This is executed via modeling the behavior of a scattered electron by the junction of a *pn* semiconductor.

First, the constant potential background is set to be $U_0 = 0$, with an associated Green's function,

$$G_0(x,x';k) = \frac{e^{ik|x-x'|}}{2ik}. \tag{7}$$

As a first approach, the two potential barriers that characterize the depletion zone are the same height, $U(x') = 0.2$eV, and width, 15Å. These barriers are defined between $[0,15]$Å and $[65,80]$Å as seen in Fig. 1. As one can observe, the potential is 0 for every other x outside the barriers.

It is worth to highlight that the grid discretization is $dx = 0.5$Å, while the depletion zone width is $\Delta = 80$Å. Thus, aliasing affects a certain range of energies due to the finite sample rate. Hence, the Nyquist-Shannon sampling theorem states that to avoid this kind of distortion, the sample rate must be at least twice the bandwidth of the signal. This leads us to look for the lower and upper energy bound without being affected by aliasing. For this purpose, equation (2) gives us the energy relation with the parameters due to, $k = 2\pi/\lambda$, where lambda is either $\lambda_d = 2\cdot dx$ or $\lambda_\Delta = 2\cdot\Delta x$. Therefore, the energy bounds are,

$$E_{lower} = \frac{\hbar^2\pi^2}{2m\,\Delta x^2} = 5.87547 \times 10^{-3}\text{eV} \tag{8}$$

* The notation term that involves the semicolon, in this case k, is not affected by any differential operator.

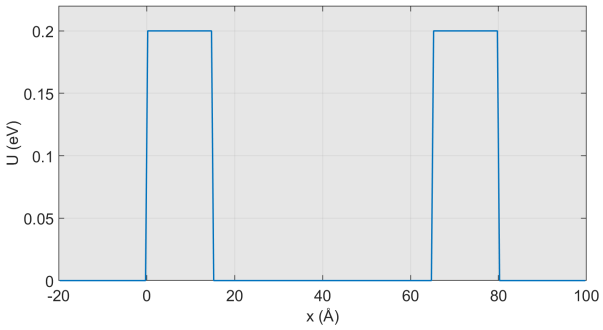

Fig. 1 Plot of the double potential barrier for the constant background in function of the grid, in Å, with the same height, 0.2 eV, and the same width, 15 Å.

for the lower bound, and,

$$E_{upper} = \frac{\hbar^2 \pi^2}{2m\, dx^2} = 150.41206\text{eV} \tag{9}$$

for the upper bound. In conclusion, the energy to avoid aliasing must be in the range of $[E_{lower}, E_{upper}] = [5.87547 \times 10^{-3}, 150.41206]$eV.

2.1 Reflection, Transmission and Absorption coefficients

Considering an incident electron as a plane wave from $x' = -\infty$ with energy, E_0, in the range $E_0 \in [0, 0.3]$eV, one can compute the reflection, $R(E_0)$, Transmission, $T(E_0)$, and Absorption, $A(E_0)$, coefficients as seen in Fig. 2.

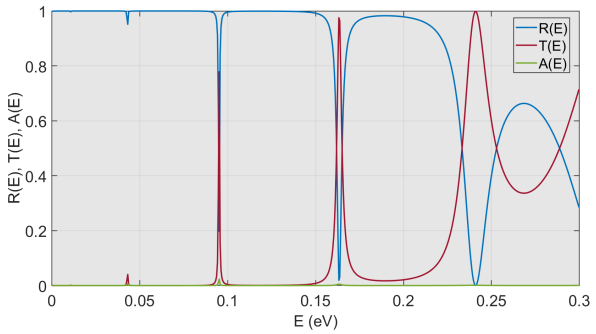

Fig. 2 Plot of the reflection, transmission, and absorption coefficients in function of energy, in eV, for the constant background potential. One can observe the different resonances and steep landscapes.

For this computation, the step is 0.0005 eV, and recombination time, $\tau = 1$ ns, which is the average lifetime of the electron before interacting with some of the recombination mechanisms of the semiconductors, e.g., Auger recombination, impurities interaction, radiative recombination, ...

2.1.1 Resonances and wavefunctions

The behavior shown in the mentioned figure is thoroughly interesting due to its resonant tunneling phenomena. This effect is the result of having the electron with the same energy (resonating) as an eigenmode in the depletion zone, such that it presents a tunneling effect while the incident energy is below the energy barrier. Once, the incident energy takes over the barrier height, then the transmission value surpasses the reflection one, yet having a last resonant behavior. However, one must take proof to stand the past affirmation to confirm that the resonant energies are indeed contained in the non-aliasing regime, $[E_{lower}, E_{upper}]$. Therefore, in these lines, we observe that all the resonances are reliable by observing the absorption coefficient in Fig. 3, which allows us to determine that they take place at $[0.01075, 0.04325, 0.09525, 0.16325, 0.23975]$ eV.

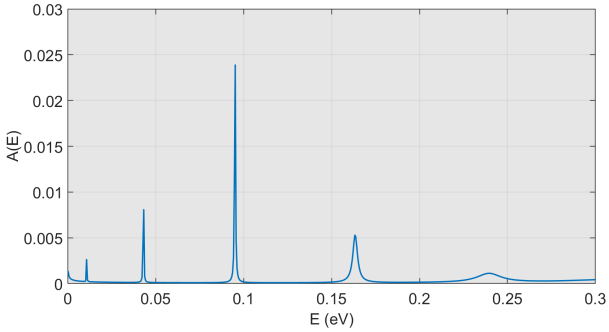

Fig. 3 Zoom in on the absorption coefficient in function of the energy, in eV, for the constant background potential. It allows to differentiate the 5 resonances and determine their energy.

Another feature to take into consideration is the widening of the peaks as one could have expected, which also validates the reliability of our results in the physical sense rather than the numerical one.

Holding these results, one is able to compute the scattering eigenstate wavefunctions which are plotted, for the sake of comparison, with the potential and a non-resonant state, although they do not have the same units. In Fig. 4, one can appreciate the predicted damping of the non-resonant state as it fades before passing through the same barrier.

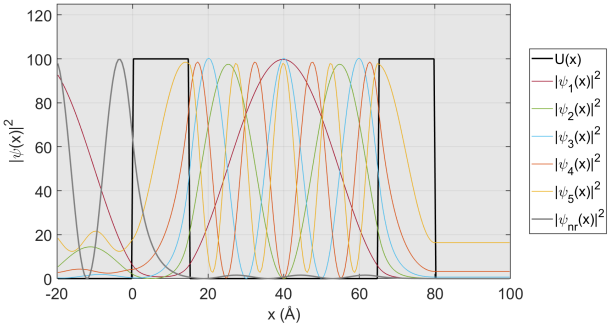

Fig. 4 Plot of the different wavefunctions for the 5 resonances, plot of one non resonant wavefunction for the average between the 3rd and 4th resonances, and plot of the potential, in function of the grid in

Å

. Everything has been rescaled as they have different units.

Moreover, it is interesting to notice how the modes depend on the wavenumber quantization k_n such that the greater n the more energy, just like it would happen in a harmonic oscillator in a

potential well for its analogous eigenmodes.

2.2 Crude approach to an applied bias

The modification consists of lowering the height of the second barrier to 0.1 eV, so as to obtain barriers with different heights. This is nothing more than facilitating the electron to pass through the depletion zone just as if an electric field is applied as it is presented in the following sections. This raw example in Fig. 5, compared to the one in Fig. 2, stresses the fact that lowering the potential height implies less steep resonances found in lower energies.

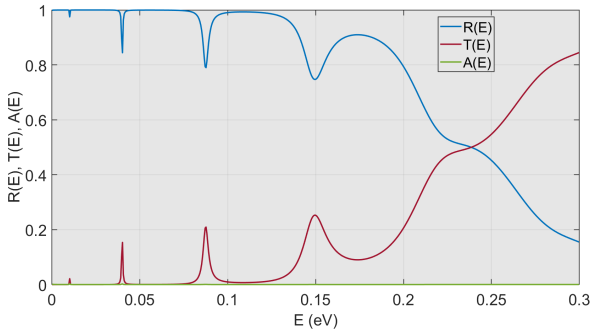

Fig. 5 Plot of the reflection, transmission, and absorption coefficients in function of energy, in eV, for the crude approach potential. One can observe the different resonances and more smooth landscapes.

Apart from that, in Fig. 6 one can notice that the absorption plot has had its resonances displaced to lower levels, one less resonance in the regime of higher energies, and the order of magnitude is reduced by a factor of ten, with respect to Fig. 3.

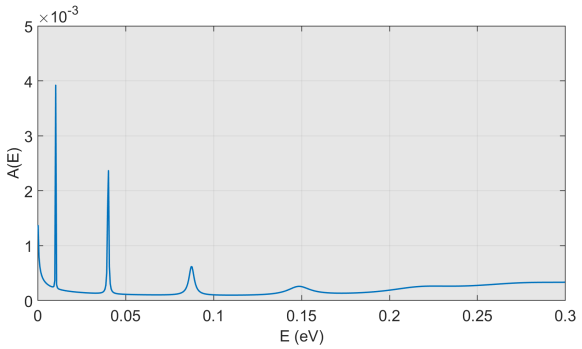

Fig. 6 Zoom in on the absorption coefficient in function of the energy, in eV, for the crude approach potential. It allows to differentiate the 4 resonances and determine their energy. Notice the order of magnitude.

3 Results for step function as reference system

The fundamental basis has been settled by studying the case of constant potential background, whereas in the following steps, the reference system is set by a step function $U_0(x<0)=0 \wedge U_0(x>0)=U_1=-0.1$ eV as potential background. Therefore, the Green's function describing the system changes, as well as, the incident wave and transmitted wave. One must take in mind that the target is to accurately describe a heterojunction of a *pn* semiconductor. For this purpose, one must take into account that it contains an electric field in the depletion zone due to the difference in the Fermi level given by the different concentrations of impurities. This is seen as a potential bias applied to the junction by means of the electric field estimated as,

$$|\mathbf{E}| = -\frac{U_1}{\Delta x'} \tag{10}$$

being $\Delta x'$ the width of the heterostructure. Thus, the potential bias applied to the initial double barrier is $U_{biased}(x') = -|\mathbf{E}|x'$ which can be appreciated in Fig. 7 modifying the initial $U(x)$.

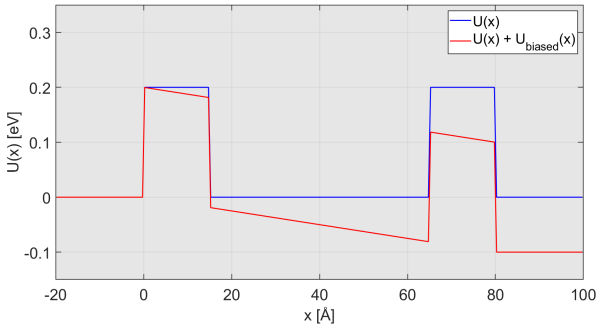

Fig. 7 Plot of the double potential barrier for the constant background (in blue) and for the biased potential (in red) in function of the grid, in Å, with the same height, 0.2 eV, and the same width, 15 Å.

Now, before computing the reflection, transmission, and absorption coefficients, one has to find the new region of non-aliased energies. In this case, the new challenge resides in the energy displacement by U_1, hence, the equation (2) leads us to $k^2 = \frac{2m_e}{\hbar^2}(E-U_1)$ where we take the real part and the relation $k = 2\pi/\lambda$. Using this result one can find the wavelengths, and with these ones, the energy boundaries are, $[\lambda_{0,min} = 22.2914, \lambda_{0,max} = 8.5287 \times 10^3]$Å and $[\lambda_{1,min} = 19.3915, \lambda_{1,max} = 38.7830 \times 10^3]$Å. All the wavelengths are contained in the expected range of depletion zone width, except the $\lambda_{0,max}$ which is much larger, thus being undetermined the transmission for very small E close to 0.

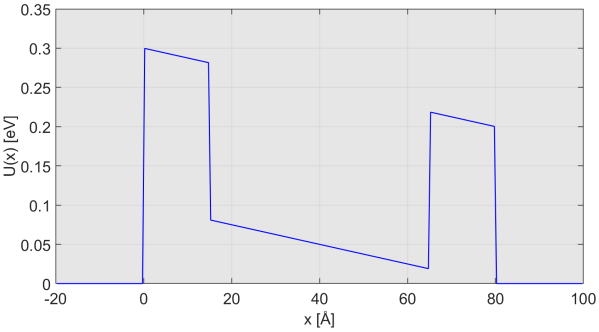

Fig. 8 Plot of the term added to a step potential for obtaining the total biased potential in function of the grid, in Å, with the same height, 0.2 eV, and the same width, 15 Å.

3.1 Reflection, Transmission and Absorption coefficients

The parameters to study the reflection, transmission, and absorption coefficients do not change from previous sections, so the energy grid is the same. What has changed is the potential, which we were using Green's function to solve for a step function. For this reason, the potential applied to (4) is the addition to the step potential plotted in Fig. 8.

Taking all those factors into account, one can compute the coefficients plotted in Fig. 9 in the same fancy as prior sections. As one can see, it represents a change from the constant background in Fig. 2, but not as drastic as the crude one in Fig. 5, which is along the lines of what was expected.

This means more steep peaks than the crude approach, with more trouble surpassing the depletion zone. However, it is easier than the one without an electric field, thus it affects the transport of charge and is more faithful to reality.

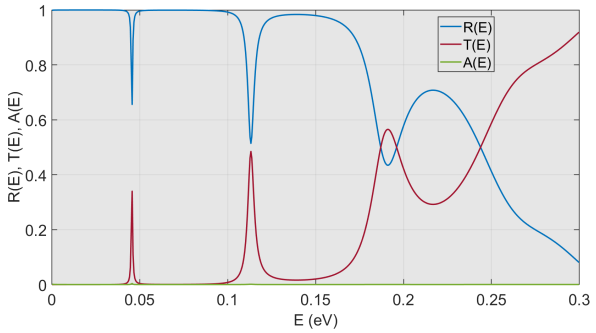

Fig. 9 Plot of the reflection, transmission, and absorption coefficients in function of energy, in eV, for the biased potential using the electric field of the depletion zone. One can observe the different resonances and steep and smooth landscapes at the same time.

3.2 Fermi level electron

Finally, for realistic dynamics of an electron at the Fermi level its energy, $E_0 = 0.01$ eV, is non-zero. Plus, the effect of tuning the bias is studied so $U_1 \in [-0.2, 0.2]$. In Fig. 10, the potentials for $U_1 = -0.2$ eV and $U_1 = 0.2$ are plotted ensemble joint with the constant reference one to envision the differences easily.

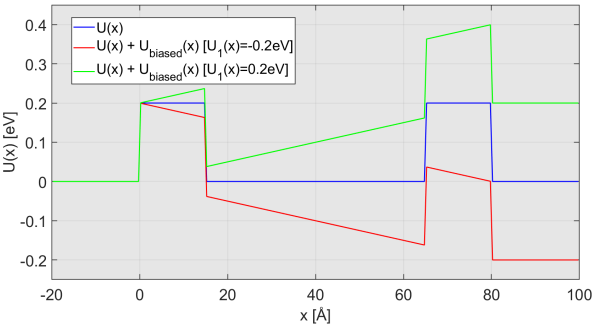

Fig. 10 Plot of the double potential barrier for the constant background (in blue), for the biased potential with $U_1 = -0.2$ eV (in red), and for the biased potential with $U_1 = 0.2$ eV (in green), in function of the grid, in Å, with the same height, 0.2 eV, and the same width, 15 Å.

Lastly, it is possible to compute the reflection, transmission, and absorption coefficients in the U_1 range considered for an electron at the Fermi level. It is plotted in Fig. 11 where the x-axis values are inverted for the sake of readability and understanding the movement of charge as positive.

4 Conclusion

For the interpretation of the phenomena, it is defined the transmission coefficient as a measure of the current due to the large amount of electrons that are contained in a heterojunction. Regarding that, there is no pass of current until some interval after 0.066 and 0.069 eV, it seemed that could either exhibit a resistance or diode behavior. The truth is that it acts as a resonant-tunneling diode (RTD) which is the effect that we have observed throughout all the work, where it tunneled through some resonant states at certain energy levels. It is a must to highlight that one can observe several negative differential resistance regions, where there is no current between what is supposed to be diode dynamics. This is a very unique characteristic that pushes forward its research to mainly ultra-high-speed operations due to the fast quantum tunneling effect through especially thin layers. Cutting-edge research involves trying to build oscillators and switching devices that can operate at terahertz frequencies.

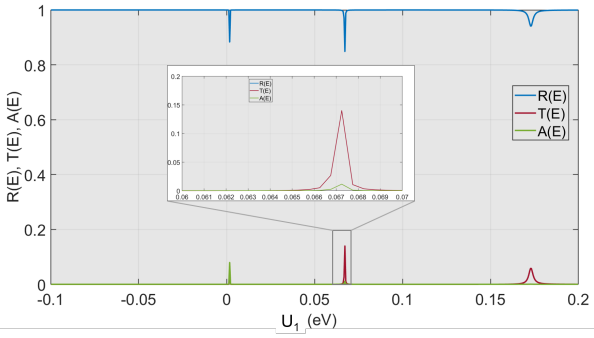

Fig. 11 Plot of the reflection, transmission, and absorption coefficients in function of inversed potential $U_1 \in [-0.2, 0-2]$ eV axis, for the biased potential using the electric field of the depletion zone. It exhibits the resonant-tunneling diode behavior due to the negative differential resistance regions.

⋆ The theoretical explanations and code script are based on the notes and lectures about Numerical Methods for the *Université de Bourgogne* by Pr. Alain Dereux.